Simulations of flow-induced director structures in nematic liquid crystals through Leslie-Ericksen equations. I. Computational methodology in two dimensions

Antonino Polimeno* and Laura Orian
Department of Physical Chemistry, University of Padova, Via Loredan 2, 35131 Padova, Italy

Assis F. Martins and Alexandre E. Gomes
Departamento de Ciência dos Materiais, Faculdade de Ciências e Tecnologia, Universidade Nova de Lisboa, P-2825-114 Monte de Caparica, Portugal

(Received 9 August 1999; revised manuscript received 21 January 2000)

A computational treatment of the constitutive equations of nematodynamics, based on the Leslie-Ericksen approach, is presented and discussed for a rotating planar nematic sample subjected to a constant magnetic field. The dynamics of the velocity **v** and director **n** fields is taken into account exactly. Coupled partial differential equations suitable to be solved numerically are worked out, in terms of derived functionals of **v** and **n** and of their spatial and time derivatives. Time-dependent patterns of the director are obtained using a finite-difference scheme in a spatial polar grid. Several experimental situations are analyzed, corresponding to common experimental setups: continuously rotating samples for different values of the rotational speed; 30° and 90° step-rotation experiments. A comparison is made to existing approximate treatments. Dependence upon the sample dimension is also discussed.

PACS number(s): 61.30.Gd, 81.10.Jt, 83.20.Jp

I. INTRODUCTION

Liquid crystals are well known examples of non-Newtonian fluids, which can be described by augmented hydrodynamic equations governing the time evolution of field variables associated with complex viscoelastic properties [1,2]. The richness of observed and/or predictable flow patterns and the desire to rationalize measurements of viscosity coefficients using a number of experimental techniques like rheology, nuclear magnetic resonance (NMR), electron spin resonance (ESR), and dielectric relaxation imply the need for a complete methodology for solving constitutive equations of liquid crystalline phases, in a way comparable to analogous numerical and analytical treatments available for Newtonian fluids based on Navier-Stokes equations.

Nematic liquid crystals (NLC's) are the first example of anisotropic fluids studied by means of hydrodynamic equations, and any computational treatment for studying the so-called nematodynamic equations is bound to be of considerable interest. First of all, a vast amount of existing experimental data is available for nematic samples, which evidently depends, for a full understanding, upon the complete computational solution of the constitutive hydrodynamic equations. Secondly, an effective computational treatment would be of importance not only for the comprehension of the dynamics of nematics themselves, but also because it might eventually be extended to more complex liquid crystalline phases, e.g., biaxial nematic, smectic *A*, or smectic *C* phases. Existing treatments of hydrodynamic equations are usually limited to stationary systems or they neglect partially or completely the backflow effects related to the coupling of director and velocity field dynamics. For these reasons, we believe that the task of solving numerically the constitutive equations for NLS's is worthwhile, despite its intrinsic complication. In this work, it is our purpose to present such a treatment at least for the case of bidimensional systems, having in mind as a first and direct application the interpretation of experimental measurements of viscoelastic coefficients in spinning samples in cylindrical tubes by means of NMR, rheo-NMR, and ESR experiments.

According to the hydrodynamic description of NLC's [3,4], the fluid is described by two vector fields in space, namely, the director unitary vector $\mathbf{n}(\mathbf{r},t)$, which gives the orientation of the director for the nematic phase at space point $\mathbf{r}$ and time t, and the velocity vector $\mathbf{v}(\mathbf{r},t)$. Constitutive Leslie-Ericksen (LE) equations [3,4] provide a closed set of partial differential relations which are in principle able to describe the fluid in both space and time, if explicit boundary and initial conditions are given, and a defect-controlled environment is assumed. We shall consider in the following a much studied case, namely, a rotating sample in the presence of a constant perpendicular magnetic field. A tube containing a nematic liquid crystal is spinning about its vertical symmetry axis, while a uniform magnetic field is turned on in a horizontal plane. Equivalent or related rheological measurements with analogous geometrical setups have been performed in the past, starting with Tsvetkov and Sosnowskii [5], who actually used a stationary sample in a rotating magnetic field. Gasparoux and Prost measured the torque exerted by the fluid on the cylinder as a function of the rotational speed [6]. Leslie, Luckhurst, and Smith performed studies on the electron spin resonance spectrum of a paramagnetic probe dissolved in the nematic [7]. Emsley, Khoo, Lindon, and Luckhurst measured the deuterium NMR spectrum for the nematic phase of a partly deuterated liquid crystal as a function of sample spinning speed [8]. Kneppe and Schneider measured the rotational viscosity coefficient of the liquid crystal [9]. Experiments related to fixed geometries of

*Corresponding author. Email address: A.Polimeno@chfi.unipd.it

the initial orientation of the director in the bulk with respect to the magnetic field have been conducted, more recently, by Martins and co-workers [10].

Recently, substantial advances in the definition and treatment of theoretical models for the comprehension of viscoelastic properties of NLC's have been made. Although this paper will be concerned only with a computational description based upon standard LE equations, it is convenient to summarize some *recent* contributions to the understanding of viscoelasticity in nematics, at both the molecular and macroscopic levels. Treatments based upon hydrodynamic models were presented in the last few years by Ziherl, Vilfan, and Žumer [11,12], to describe director fluctuation in confined systems. Mechanical stability conditions in the annular geometry of a NLC sample were studied by, among others Palffy-Muhoray, Sparavigna, and Strigazzi [13] and by Kiselev and Reshetnyak [14]. Flow properties, also in connection with surface anchoring energy, were considered, from different points of view, by Tsuji and Rey [15], Dolmatova and Kozhevnikov [16], and Porte, Berret, and Harden [17]. Simulations based on the LE equations of bipolar droplets were carried out by Chan and Rey [18], while approximated numerical treatments of the LE equations for rotating planar NLC's were recently presented by Polimeno and Martins [19]. Molecular interpretations of viscosity coefficients have been given, for instance, by Larson and Archer [20], Chrzanowska and Sokalski [21], Zubarev and Iskakova [22], Kroger and Sellers [23] and Fialkowski [24]. General viscoelastic theoretical investigations are due to Volino and co-workers [25].

Direct measurements of viscoelastic parameters in NLC's have also been increasing in number. Imai *et al.* employed transient current techniques to determine rotational viscosities of NLC display devices [26]; Cipparrone *et al.* used optical measurements [27]; Mather *et al.* investigated stress-oscillation damping with polarized light [28]. Rheological investigations of viscoelastic micellar solutions were conducted by Cappelaere and Cressely [29], while Berret studied wormlike micelles [30], and Sequeira and Hill considered particle suspensions in nematics [31]. Electrorheological experiments were conducted, for instance, by Kuhnau, Schmiedel, and Stannarius [32] and by Yao and Jamieson [33]. Magnetic field effects used in connection with rheological measurements are currently much employed by many researchers. Recent data on low molecular weight NLC's obtained with NMR proton techniques are given, for instance, by Gotzig, Grunenberghassanein, and Noack [34] and Grigutsch *et al.* [35]. Extensive studies on rotating samples with negative anisotropy of magnetic susceptibility were recently performed by Ciampi and Emsley [36]. Viscoelastic properties of biomembranes have been studied by Althoff *et al.* [37], while polymer nematics were studied by Martins and co-workers [10,38] and Diao and Berry [39].

Despite the relevant amount of theoretical and experimental work concerning flow properties of NLC's, a thorough analysis of patterns obtained within the framework of the LE equations, when the full coupling between velocity and director fields is taken into account, appears to be still missing [40]. Backflow effects are especially important when sudden rotation impulses are impressed on NLC samples, and a better understanding of simulated director patterns could greatly help the determination of viscoelastic parameters, using any of the experimental techniques already mentioned. Very recently, we have started a systematic exploration of dynamical regimes predicted by numerical solutions of the LE equations in planar NLC samples. Preliminary solutions [19] were presented for approximate treatments of systems in stationary rotation, without backflow effects and imposing a defect in the center of the sample. Here we intend to present a more advanced treatment of the LE equations, which is essentially exact, within the limitation of having the sample confined to a two-dimensional geometry.

The paper is organized as follows. In the next section the LE equations are briefly summarized and discussed. In Sec. III algebraic manipulations are introduced to cast them in a form amenable to computational solutions, and the actual computational methodology is presented for calculating transient director patterns. Results concerning spatial and angular distributions of the director field are discussed in Sec. IV for a standard low molecular weight NLC. Finally, a brief Discussion is included to summarize our findings.

II. LESLIE-ERICKSEN EQUATIONS

The Leslie-Ericksen equations for an incompressible nematic are summarized in this section [3,4]:

$$[\hat{\nabla}\cdot\boldsymbol{\sigma}]=\rho\frac{d\mathbf{v}}{dt}, \tag{1}$$

$$\mathbf{G}+\mathbf{g}+[\hat{\nabla}\cdot\boldsymbol{\pi}]=0, \tag{2}$$

where in the velocity equation (1) the unknown vector $\mathbf{v}(\mathbf{r},t)$ is the velocity field of the fluid at point $\mathbf{r}$ and time t, ρ is the bulk density, $\boldsymbol{\sigma}$ is the stress tensor, and body forces have been neglected; in the director equation (2) the unknown unitary vector $\mathbf{n}(\mathbf{r},t)$ is the director field of the fluid at point $\mathbf{r}$ and time t, $\mathbf{G}$ is the external force acting on the director, $\mathbf{g}$ is the internal director body force, and $[\hat{\nabla}\cdot\boldsymbol{\pi}]$ is an elastic term. Notice that inertial terms have been neglected in the director equation. The material time derivative is defined as $d/dt=\partial/\partial t+\mathbf{v}\cdot\hat{\nabla}$; if $\mathbf{M}$ is a generic matrix we define $[\hat{\nabla}\cdot\mathbf{M}]_i=M_{ji,j}$. The stress matrix $\boldsymbol{\sigma}$ is written as

$$\sigma_{ji}=-p\,\delta_{ji}-\pi_{jk}n_{k,i}+\sigma'_{ji}, \tag{3}$$

$$\sigma'_{ji}=\alpha_1 n_k n_p A_{kp} n_j n_i+\alpha_2 n_j N_i+\alpha_3 n_i N_j+\alpha_4 A_{ji}+\alpha_5 n_j n_k A_{ki}+\alpha_6 n_i n_k A_{kj}. \tag{4}$$

The internal director body force $\mathbf{g}$ is

$$g_i=\lambda_L n_i-\frac{\partial W}{\partial n_i}-\gamma_1 N_i-\gamma_2 A_{ik}n_k, \tag{5}$$

where the following vectors and matrices are defined in terms of the components of the velocity and director field, and of derivatives of the elastic energy W:

$$A_{ji}=\tfrac{1}{2}(v_{j,i}+v_{i,j}), \tag{6}$$

$$\omega_{ji}=\tfrac{1}{2}(v_{j,i}-v_{i,j}), \tag{7}$$

$$N_i=\frac{dn_i}{dt}-\omega_{ik}n_k, \tag{8}$$

$$\pi_{ji}=\frac{\partial W}{\partial n_{i,j}}. \tag{9}$$

The elastic energy itself is defined as

$$W=\tfrac{1}{2}K_{11}(\hat{\nabla}\cdot\mathbf{n})^2+\tfrac{1}{2}K_{22}(\mathbf{n}\cdot\hat{\nabla}\times\mathbf{n})^2+\tfrac{1}{2}K_{33}(\mathbf{n}\times\hat{\nabla}\times\mathbf{n})^2 \tag{10}$$

in the spherical approximation ($K_{11}=K_{22}=K_{33}\equiv K$) the elastic energy is reduced to $W=Kn_{i,j}n_{i,j}/2$. The coefficients α_i ($i=1,\ldots,6$), γ_1, and γ_2 in expressions (4) and (5) are viscosity coefficients; the following relations hold:

$$\gamma_1=\alpha_3-\alpha_2, \tag{11}$$

$$\gamma_2=\alpha_3+\alpha_2=\alpha_6-\alpha_5, \tag{12}$$

$$\gamma_3=\alpha_6+\alpha_5. \tag{13}$$

From Eq. (12) one can see that there are only five independent viscosity coefficients [1,2]. Finally, the functions $p(\mathbf{r},t)$ (pressure) and $\lambda_L(\mathbf{r},t)$ are indeterminate Lagrange multipliers deriving from the constraints

$$\hat{\nabla}\cdot\mathbf{v}=0, \tag{14}$$

$$\mathbf{n}\cdot\mathbf{n}=1. \tag{15}$$

As outlined in the Introduction, in this work we shall be concerned with the application of LE equations to the interpretation of dynamical patterns developed by the director field in samples of nematic liquid crystals in tubes subjected to magnetic fields and to some given profile of rotation. A point in space is identified by the vector $\mathbf{r}$, which is defined by the Cartesian coordinates (r_1,r_2,r_3), or by the cylindrical coordinates (r,θ,z). The laboratory frame is defined by the three unitary vectors $\mathbf{e}_1$, $\mathbf{e}_2$, and $\mathbf{e}_3$. The radius of the cylinder is R. The magnetic field is defined as $\mathbf{H}=H\mathbf{e}_1$. The external director body force is given simply by $\mathbf{G}=\chi_a(\mathbf{H}\cdot\mathbf{n})\mathbf{H}=\chi_a H^2 n_1\mathbf{e}_1$, where $\chi_a=\chi_\parallel-\chi_\perp$ ($\chi_\parallel$ and $\chi_\perp$ are the principal diamagnetic susceptibilities per unit volume). The rotating cylinder is subjected to a rotational motion around the $\mathbf{e}_3$ axis with a generic time-dependent speed, which will be defined in the following as $\Omega f(t)$, where Ω has the dimension of an angular velocity and $f(t)$ is a function of time specifying the profile of the rotational impulse to which the vessel is submitted. In the case of constant rotational velocity, $f(t)=1$. In this case (stationary rotation) one can use an approximate treatment based on the assumption that the velocity field $\mathbf{v}(\mathbf{r},t)$ of the rotating nematic is equal to the steady-state velocity field of a Newtonian fluid, i.e., the velocity equation is simplified by assuming a Newtonian fluid form for the stress tensor [41,42] $\boldsymbol{\sigma}=-p\mathbf{1}-\alpha_4\mathbf{A}$, and the steady-state condition $\partial\mathbf{v}/\partial t=\mathbf{0}$. It follows that, for a cylindrical symmetry, the z and r components of the velocity field vector are zero, $v_z=v_r=0$, and the θ component v_θ is obtained from the equation

$$\alpha_4\frac{\partial}{\partial r}\frac{1}{r}\frac{\partial}{\partial r}rv_\theta=0, \tag{16}$$

taking into account that the pressure gradient is zero along θ for a steady-state Newtonian cylindrical sample. By assuming that at the boundaries the fluid follows the rotating cylinder, one gets the well known result $v_\theta=\Omega r$ or $\mathbf{v}=\boldsymbol{\Omega}\times\mathbf{r}$, i.e., the fluid is behaving as a rigid body. Notice that in Eq. (16) the dependence upon the viscosity coefficient α_4 disappears due to the steady-state condition [19].

III. A COMPLETE TREATMENT FOR PLANAR SAMPLES

We shall consider in this section the definition of a set of refined equations for the treatment of cylindrical rotating nematic samples, without significant additional approximations, besides assuming a bidimensional geometry. The following assumptions will be made in the rest of this section.

Assumption I. In an infinitely long cylinder, if no external flows are imposed along the $\mathbf{e}_3$ axis, the dependence of $\mathbf{v}$ and $\mathbf{n}$ upon the r_3 coordinate may be neglected.

Assumption II. Components of $\mathbf{n}$ and $\mathbf{v}$ along the $\mathbf{e}_3$ axis are set to zero.

A less relevant approximation, namely, the spherical treatment of the elastic tensor, will be made mostly for sake of simplicity. Inclusion of the complete elastic tensor is straightforward, however. We start to consider the velocity equation (1), and we rewrite explicitly the tensor $\boldsymbol{\sigma}$:

$$\boldsymbol{\sigma}=-p\mathbf{1}+\boldsymbol{\sigma}^e+\boldsymbol{\sigma}', \tag{17}$$

where $\sigma^e_{ji}=-\pi_{jk}n_{k,i}$. According to assumptions I and II, the velocity field can be written in terms of the *streamlines function* $\Psi(r_1,r_2,t)$ [41,42]:

$$\mathbf{v}=\begin{pmatrix} -\dfrac{\partial\Psi}{\partial r_2} \\ +\dfrac{\partial\Psi}{\partial r_1} \\ 0 \end{pmatrix}. \tag{18}$$

A partial differential equation in Ψ can be obtained by differentiating the first of the velocity equations by $\partial/\partial r_1$, the second one by $\partial/\partial r_2$, and subtracting. The resulting equation is

$$\hat{\nabla}^2\Psi=\Xi, \tag{19}$$

$$\frac{\partial\Xi}{\partial t}+\frac{\partial(\Psi,\Xi)}{\partial(r_1,r_2)}=\mathcal{F} \tag{20}$$

(expressed for simplicity in Cartesian coordinates), where the function Ξ, which is essentially the vorticity of the fluid, is conveniently introduced. Notice that for generic a,b,α,β the following notation holds:

$$\frac{\partial(a,b)}{\partial(\alpha,\beta)}=\det\begin{pmatrix} \dfrac{\partial\alpha}{\partial\alpha} & \dfrac{\partial a}{\partial\beta} \\ \dfrac{\partial b}{\partial\alpha} & \dfrac{\partial b}{\partial\beta} \end{pmatrix}. \tag{21}$$

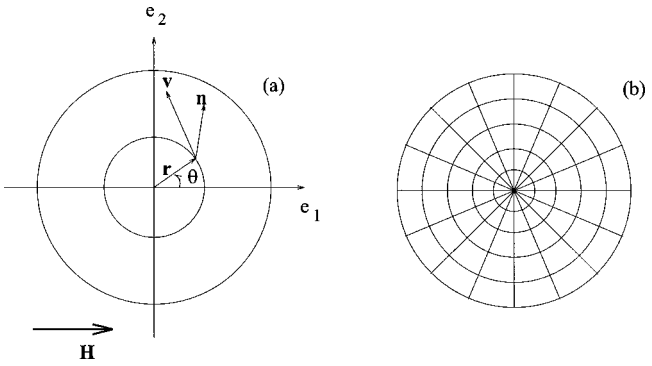

FIG. 1. Section of a cylindrical nematic sample, in scaled coordinates. A sample point is defined by cartesian scaled coordinates $-1\leqslant x_1\leqslant 1$ and $-1\leqslant x_2\leqslant 1$, or by polar coordinates $0\leqslant x\leqslant 1$ and $0\leqslant\theta\leqslant 2\pi$. The polar grid employed in the numerical solution of LE equations is also shown.

$\mathcal{F}$ is a function of derivatives of Ψ,Ξ and of the director orientation. The derivation of function $\mathcal{F}$ is lengthy but straightforward. Here we summarize the main results. The function $\mathcal{F}$ depends upon the stress tensor in the following way:

$$\mathcal{F}=\frac{1}{\rho}\left[-\frac{\partial}{\partial r_2}\left(\frac{\partial\sigma_{11}}{\partial r_1}+\frac{\partial\sigma_{21}}{\partial r_2}\right)+\frac{\partial}{\partial r_1}\left(\frac{\partial\sigma_{12}}{\partial r_1}+\frac{\partial\sigma_{22}}{\partial r_2}\right)\right]. \tag{22}$$

It is convenient to consider separately each contribution coming from the viscous stress tensor, which we shall write in the form

$$\sigma_{ji}=\sigma^e_{ji}+\sigma^1_{ji}+\sigma^{2,3}_{ji}+\sigma^4_{ji}+\sigma^{5,6}_{ji}-p\,\delta_{ji}, \tag{23}$$

$$\sigma^e_{ji}=-\pi_{jk}n_{k,l}, \tag{24}$$

$$\sigma^1_{ji}=\alpha_1 n_k n_p A_{kp} n_j n_i, \tag{25}$$

$$\sigma^{2,3}_{ji}=\alpha_2 n_j N_i+\alpha_3 n_i N_j, \tag{26}$$

$$\sigma^4_{ji}=\alpha_4 A_{ji}, \tag{27}$$

$$\sigma^{5,6}_{ji}=\alpha_5 n_j n_k A_{ki}+\alpha_6 n_i n_k A_{kj}, \tag{28}$$

so that the $\mathcal{F}$ function is obtained as the sum of the corresponding terms,

$$\mathcal{F}=\mathcal{F}^e+\mathcal{F}^1+\mathcal{F}^{2,3}+\mathcal{F}^4+\mathcal{F}^{5,6}, \tag{29}$$

without any explicit dependence upon the pressure p. Let us first consider the elastic contribution. In the spherical approximation, the tensor π_{ji} is simply $\pi_{ji}=Kn_{i,j}$. It follows that the elastic contribution $\mathcal{F}$ can be obtained in the form

$$\mathcal{F}^e=\frac{K}{\rho}\frac{\partial(\phi,\hat{\nabla}^2\phi)}{\partial(r_1,r_2)}, \tag{30}$$

where $\phi(r_1,r_2,t)$ is the angle specifying the director orientation (see Fig. 1). Next we consider the term proportional to α_1:

$$\mathcal{F}^1=\frac{\alpha_1}{\rho}\left[-\frac{\partial^2}{\partial r_1\partial r_2}M\cos 2\phi+\frac{1}{2}\left(\frac{\partial^2}{\partial {r_1}^2}-\frac{\partial^2}{\partial {r_2}^2}\right)M\sin 2\phi\right], \tag{31}$$

$$M=\frac{1}{2}\sin 2\phi\left(\frac{\partial^2\Psi}{\partial {r_1}^2}-\frac{\partial^2\Psi}{\partial {r_2}^2}\right)-\cos 2\phi\,\frac{\partial^2\Psi}{\partial r_1\partial r_2}. \tag{32}$$

The α_2,α_3 term can be calculated after defining the ancillary function $\Sigma=n_1N_2-n_2N_1$. By inspection one can see that

$$\Sigma=\frac{\partial\phi}{\partial t}+\frac{\partial(\Psi,\phi)}{\partial(r_1,r_2)}-\frac{1}{2}\Xi, \tag{33}$$

$$\mathcal{F}^{2,3}=\frac{\gamma_2}{\rho}\left[\frac{\partial^2}{\partial r_1\partial r_2}\Sigma\sin 2\phi+\frac{1}{2}\left(\frac{\partial^2}{\partial {r_1}^2}-\frac{\partial^2}{\partial {r_2}^2}\right)\Sigma\cos 2\phi\right]-\frac{\gamma_1}{2\rho}\hat{\nabla}^2\Sigma. \tag{34}$$

The α_4 term is the simple Newtonian (Navier-Stokes) term [41,42]

$$\mathcal{F}^4=\frac{\alpha_4}{2\rho}\hat{\nabla}^2\Xi. \tag{35}$$

Notice that if only this contribution is retained the velocity is uncoupled from the director orientation, i.e., no effects on the velocity dynamical behavior are predicted due to the director reorientation (*backflow*). Finally, the α_5,α_6 term is obtained by similar algebraic manipulations in the form

$$\mathcal{F}^{5,6}=\frac{\gamma_3}{4\rho}\hat{\nabla}^2\Xi-\frac{\gamma_2}{2\rho}\hat{\nabla}^2N, \tag{36}$$

$$N=\frac{1}{2}\cos 2\phi\left(\frac{\partial^2\Psi}{\partial {r_1}^2}-\frac{\partial^2\Psi}{\partial {r_2}^2}\right)-\sin 2\phi\,\frac{\partial^2\Psi}{\partial r_1\partial r_2}. \tag{37}$$

Next we shall consider the time-dependent orientation of the director field. The two nonzero components of the director unitary vector are conveniently expressed as

$$\mathbf{n}=\begin{pmatrix}\cos\phi\\ \sin\phi\\ 0\end{pmatrix}. \tag{38}$$

Our starting equation is the equation of motion of the director, which can be written as

$$\chi_a H^2 n_1\mathbf{e}_1+\mathbf{g}+[\hat{\nabla}\cdot\boldsymbol{\pi}]=0. \tag{39}$$

The director equation can be conveniently manipulated by multiplying the first and second components by n_2 and n_1, respectively, and subtracting:

$$\chi_a H^2 n_1 n_2+n_2 g_1-n_1 g_2+n_2[\hat{\nabla}\cdot\boldsymbol{\pi}]_1-n_1[\hat{\nabla}\cdot\boldsymbol{\pi}]_2=0. \tag{40}$$

In the spherical approximation the elastic term is simply given by $n_2[\hat{\nabla}\cdot\boldsymbol{\pi}]_1-n_1[\hat{\nabla}\cdot\boldsymbol{\pi}]_2=-K\hat{\nabla}^2\phi$ [19]. The magnetic term assumes the form $\chi_a H^2\sin 2\phi/2$, whereas the more complicated viscous part depends upon second deriva-

tives of Ψ with respect to r_1 and r_2. Several manipulations allow us now to obtain an explicit equation in Ψ, ϕ. Skipping unnecessary details, one is left with the following expression:

$$\frac{\partial \phi}{\partial t}+\frac{\partial(\Psi,\phi)}{\partial(r_1,r_2)}=\mathcal{G}. \tag{41}$$

The final expression for the $\mathcal{G}$ function is given by

$$\mathcal{G}=\frac{1}{2}\Xi-\frac{\chi_a H^2}{2\gamma_1}\sin 2\phi+\frac{K}{\gamma_1}\hat{\nabla}^2\phi-\frac{\gamma_2}{\gamma_1}\left[\sin 2\phi\,\frac{\partial^2\Psi}{\partial r_1\partial r_2}+\frac{1}{2}\cos 2\phi\left(\frac{\partial^2\Psi}{\partial {r_1}^2}-\frac{\partial^2\Psi}{\partial {r_2}^2}\right)\right]. \tag{42}$$

The final equations for the treatment of a nematic sample in two dimensions in the presence of a magnetic field are thus given by Eqs. (19)–(37) and (41) and (42).

A. Scaled equations

For practical implementation it is convenient to define scaled functions $\xi=\Xi/\Omega$, $\psi=\Psi/\Omega R^2$, and scaled time and coordinates, $\tau=t\Omega$, $x_1=r_1/R$, $x_2=r_2/R$; here Ω has the dimension of a rotational velocity. Scaled velocity field components are simply $v_1/\Omega R$ and $v_2/\Omega R$. The system of coupled equations assumes the following, rather complex, form:

$$\frac{\partial \phi}{\partial \tau}+\frac{\partial(\psi,\phi)}{\partial(x_1,x_2)}-\frac{1}{2}\xi=\varsigma, \tag{43}$$

$$\frac{\partial \xi}{\partial \tau}+\frac{\partial(\psi,\xi)}{\partial(x_1,x_2)}=a_K\frac{\partial(\phi,\hat{\nabla}^2\phi)}{\partial(x_1,x_2)}+a_1\left[-\frac{\partial^2}{\partial x_1\partial x_2}\mu\cos 2\phi+\frac{1}{2}\left(\frac{\partial^2}{\partial {x_1}^2}-\frac{\partial^2}{\partial {x_2}^2}\right)\mu\sin 2\phi\right]+a_2\left[\frac{\partial^2}{\partial x_1\partial x_2}\varsigma\sin 2\phi+\frac{1}{2}\left(\frac{\partial^2}{\partial {x_1}^2}-\frac{\partial^2}{\partial {x_2}^2}\right)\times\varsigma\cos 2\phi\right]+a_3\hat{\nabla}^2\varsigma+a_4\hat{\nabla}^2\xi+a_5\hat{\nabla}^2\nu, \tag{44}$$

$$\xi=\hat{\nabla}^2\psi, \tag{45}$$

$$\varsigma=\lambda\eta+b_1\sin 2\phi+b_2\hat{\nabla}^2\phi, \tag{46}$$

$$\eta=\frac{1}{2}\cos 2\phi\left(\frac{\partial^2\psi}{\partial {x_1}^2}-\frac{\partial^2\psi}{\partial {x_2}^2}\right)+\sin 2\phi\,\frac{\partial^2\psi}{\partial x_1\partial x_2}, \tag{47}$$

$$\mu=\frac{1}{2}\sin 2\phi\left(\frac{\partial^2\psi}{\partial {x_1}^2}-\frac{\partial^2\psi}{\partial {x_2}^2}\right)-\cos 2\phi\,\frac{\partial^2\psi}{\partial x_1\partial x_2}, \tag{48}$$

$$\nu=\frac{1}{2}\cos 2\phi\left(\frac{\partial^2\psi}{\partial {x_1}^2}-\frac{\partial^2\psi}{\partial {x_2}^2}\right)-\sin 2\phi\,\frac{\partial^2\psi}{\partial x_1\partial x_2}. \tag{49}$$

Coefficients a_K, a_i $(i=1,\cdots,5)$, λ, and b_j $(j=1,2)$ are not all independent and they can be written explicitly in terms of the viscoelastic constants: $a_K=K/s^2\rho$, $a_1=\alpha_1/s\rho$, $a_2=\gamma_2/s\rho$, $a_3=-\gamma_1/2s\rho$, $a_4=(\alpha_4/2+\gamma_3/4)/s\rho$, and $a_5=-\gamma_2/2s\rho=-a_2/2$ where $s=\Omega R^2$; and $\lambda=-\gamma_2/\gamma_1$, $b_1=-\chi_a H^2/2\gamma_1\Omega$, and $b_2=K/\gamma_1 s$. Notice that coefficients a_i are essentially Ekman numbers and b_2 is the inverse of a rotational Ericksen number.

B. Boundary and initial conditions

Definition of boundary and initial conditions is indispensable for completing the implementation of the hydrodynamic treatment and for comparing simulated results with available experimental data, which are informative, albeit in an indirect way, about the main features of the director distribution in rotating samples, both for start-and-stop and continuously rotating setups [7,8,10]. Nevertheless, a precise definition of the beahvior of the fluid at the nematic-solid interface is difficult, and dependent upon the experimental situation. Since our purpose in this work is to underline an efficient methodology for treating nematics effectively and to interpret qualitatively the main features observed in magnetic resonance and rheological experiments, we shall dispense with an accurate definition of boundary conditions based on refined microscopic or macroscopic treatments and assume very simple descriptions of the director and velocity fields at the interface.

First of all, we shall set the velocity field equal to the rotational velocity of the cylinder in the vicinity of the internal walls. In terms of the ϕ and ξ functions, one can write $\psi(\tau)\to f(\tau)x^2/2$ and $\xi(\tau)\to 2f(\tau)$ for $x\to 1$, where $x=\sqrt{x_1^2+x_2^2}$ is the scaled radial coordinate $0\leqslant x\leqslant 1$ and $f(\tau)$ is the scaled form of $f(t)$, defined in Sec. II above. These are the well known boundary conditions assumed for Newtonian fluids in rotating tubes [42].

Simplified boundary conditions for the director can be imposed essentially in two ways: One can assume that regardless of the fluid rotation the orientation of the director in the proximity of the walls is constant. This is the case of strong anchoring, i.e., Dirichlet boundary conditions, $\phi(\tau)\to$const for $x\to 1$. On the other extreme, we can assume that in the neighborhood of the internal walls the LE equations are satisfied without significant changes of the director orientation due to interaction with the walls. This is the case of zero anchoring $\partial\phi(\tau)/\partial x\to 0$ for $x\to 1$, or Neumann boundary conditions. We shall consider in the following only zero-anchoring conditions, i.e., we shall assume that the behavior of the nematic in the rotating sample, in a boundary layer close to internal walls of the cylindrical container, is essentially independent of interaction with the walls. This choice is clearly not realistic if one considers the case of a nonrotating tube whose internal surface has been treated to align the director along some easy axis, but it can be accepted as a rough description for a fast rotating surface, for which the major contribution to the free energy of the nematic in the boundary layer comes from the kinetic term. Measurements of azimuthal (in the plane) anchoring free energy per unit area give values smaller than 10^{-3} J m^2 [43], whereas for the cases treated in the following sections the free kinetic energy could be estimated one or two orders of magnitude larger.

TABLE I. Parameters employed in the simulations.

Density	ρ	10^3 kg m^{-3}
Susceptibility	χa	1×10^{-7}
Field	H	0.3349 T
Average elastic constant	K	1×10^{-11} N
Leslie coefficients	α_i	-0.0087, -0.052, -0.002, 0.058, 0.038, -0.016 Pa s
Critical velocity	Ω_c	1.12 s^{-1}

However, it is clear that a more accurate description of the interaction between director and walls, using a suitable functional for the free energy of the director at the boundary layer, should be employed for a realistic description of the interface. In this work, mainly devoted to exploration of the computational methodology for treating the hydrodynamical behavior of a nematic fluid in two dimensions, we shall not investigate the effects of different descriptions of the interface, reserving an analysis of the problem to future studies.

Notice that by assuming no spatial dependence in the whole sample for the director field and Newtonian behavior of the velocity field one recovers the following simplified law for the director orientation at the walls:

$$\frac{d\phi(\tau)}{d\tau} = f(\tau) + b_1 \sin\phi(\tau), \quad x \to 1, \tag{50}$$

which is, not surprisingly, the simplified equation obtained for the director orientation in previous standard treatments [1] that neglect space dependence. Initial conditions will be defined in all the following calculations assuming that at $\tau = 0$ boundary conditions are extended to the whole sample; i.e., since $f(0)=0$, one can simply assume that at the beginning the system is at rest ($\psi=\xi=0$) and perfectly aligned with the magnetic field ($\phi=0$).

C. Computational procedure

The methodology chosen to solve numerically the system of partial differential equations outlined in the previous sections is straightforward, and it is described as follows. We have adopted on purpose a strategy based on robustness and simplicity, at the price of a certain loss of computational efficiency in terms of storage memory and CPU time. Refinements to speed up the codes and make them less demanding on computer resources are currently being investigated.

Our approach is then based on a simple finite-difference algorithm; for symmetry reasons, it is convenient to use a polar grid (see Fig. 1) in the circular region of the sample. The scaled equations are then discretized in space, using straightforward extensions of constant step difference schemes, with increased accuracy. We have explored grids up to 1500 points, and all the simulations presented here were performed with a grid of 801 points, i.e., 20 points

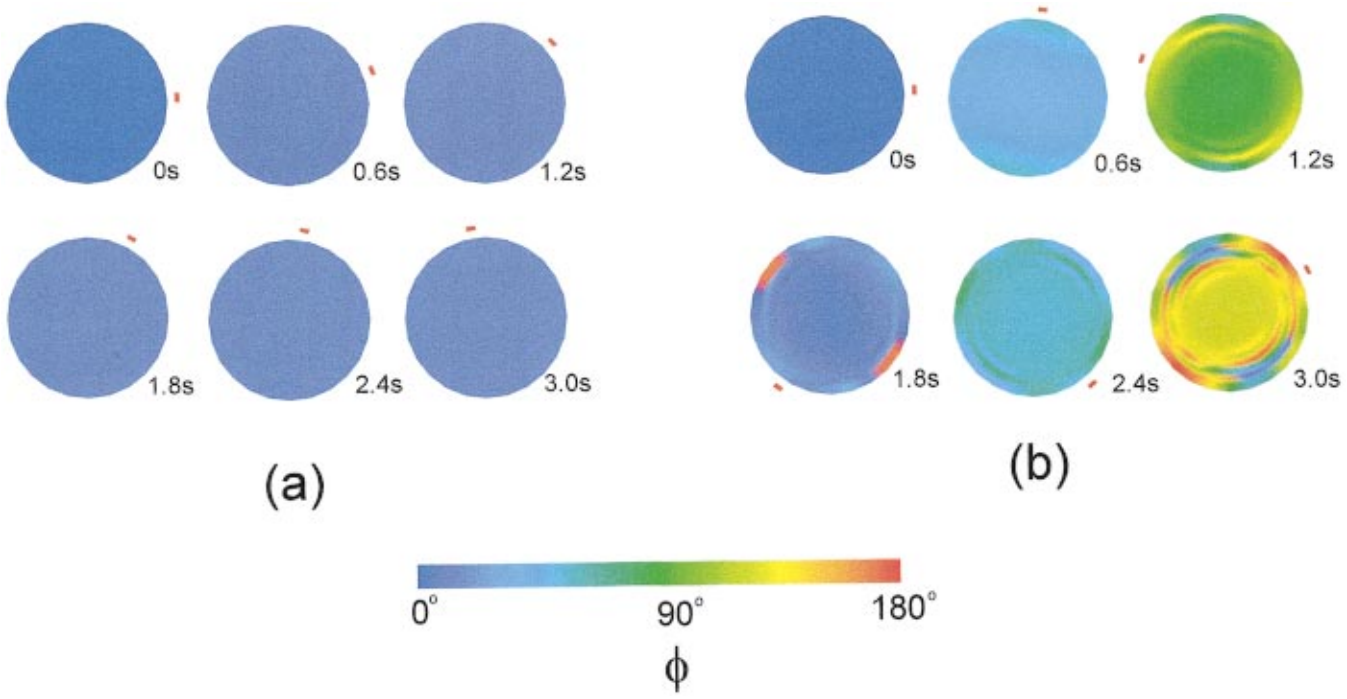

FIG. 2. (Color) Director patterns at different times for continuous rotation at $\Omega=\Omega_c/2$ (a) and $2\Omega_c$ (b). Each circle shows the director pattern in the nematic sample at a given time, in scaled coordinates (cf. Fig. 1), using a false color representation of the director angle ϕ in each point of the sample. The red dot represents the amount of rotation of the tube at the same time. The shots are shown for times 0, 0.6, 1.2, 1.8, 2.4, and 3 s; for a sample of radius $R=5$ mm.

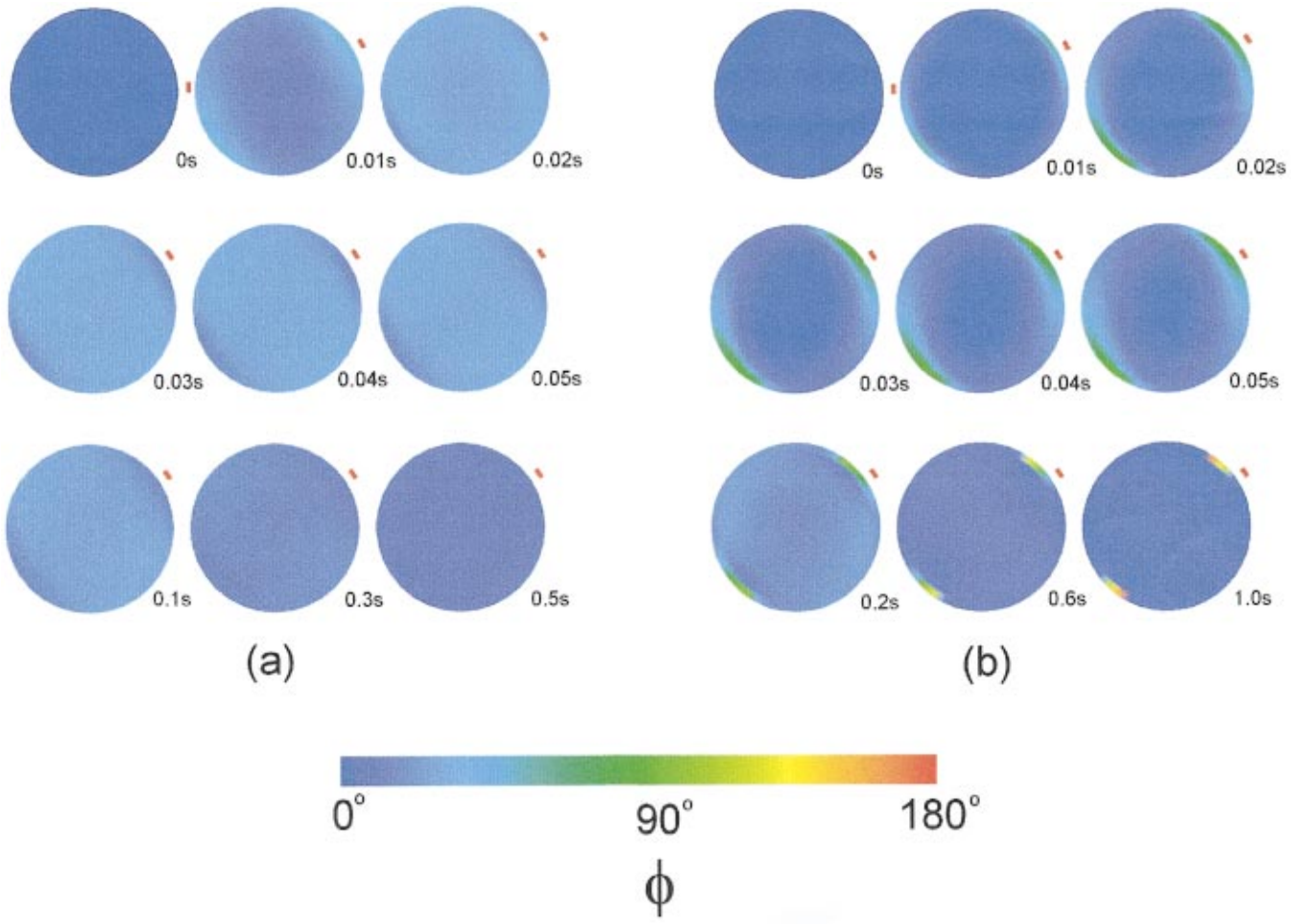

FIG. 3. (Color) Director patterns at different times for step-rotation pulses of 30° for $R=1$ mm (a) and 5 mm (b). Each circle shows the director pattern in the nematic sample at a given time, in scaled coordinates (cf. Fig. 1), using a false color representation of the director angle ϕ in each point of the sample. The red dot represents the amount of rotation of the tube at the same time. The shots are shown for times 0, 0.01, 0.02, 0.03, 0.04, 0.05, 0.1, 0.3, and 0.5 s for the case of $R=1$ mm and 0, 0.01, 0.02, 0.03, 0.04, 0.05, 0.2, 0.6, and 1.0 s for the case of $R=5$ mm.

(angular coordinate)$\times 40$ points (radial coordinate) plus the center.

Time is treated using an implicit scheme with an adjustable step, employing a standard solver for stiff systems of ordinary differential equations. For each time step, the primary functions ϕ and ξ are known; first one evaluates accurately spatial derivatives of ϕ,ξ and solves the Poisson equation in ψ (this being a particularly simple operation in the chosen grid); then derivatives of ψ are calculated, together with ancillary functions ς, η, μ, and ν. The time derivatives of ϕ and ξ are thus calculated. The whole procedure is then repeated at the following time step. The computational CPU time is relatively high: on a Silicon Graphics Octane a full simulation (see below for actual data) takes a time ranging from 3 to 5 h.

IV. CALCULATED RESULTS

We shall illustrate in this work results related to a fixed set of viscoelastic parameters, chosen to represent a low-viscosity standard nematic (see Table I): Leslie coefficients are chosen to be of the order of 0.1 Pa s [44], the average elastic constant is taken to be 1×10^{-11} N, the magnetic susceptibility and the density are chosen to have typical values like 1×10^{-7} and 10^3 kg/m^3. These values were chosen having in mind the nematogen *N*-(*p*-methoxybenzylidene)-*p*-butylalanine (MBBA) 10 K below its clearing point. The magnetic field is chosen to have a value characteristic for a standard ESR experiment, 0.3349 T.

In order to quantify the coupling strength of the magnetic field with the director vector, it is useful to employ a derived parameter, the so-called critical velocity Ω_c, which is calculated from the simplified standard treatment of a continuously rotating sample, when spatial dependence and time dependence are completely neglected [1,7]. In this case, the condition for a stationary (homogeneous) director orientation is given simply by

$$\sin 2\phi = \frac{\Omega}{\Omega_c}, \tag{51}$$

where $\Omega_c=\chi_a H^2/2\gamma_1$. Only if $\Omega<\Omega_c$ does the simplified treatment predict a stationary distribution. We shall see that predictions of the simplified treatment are obeyed roughly by the actual simulations, at least for the case of a sample in

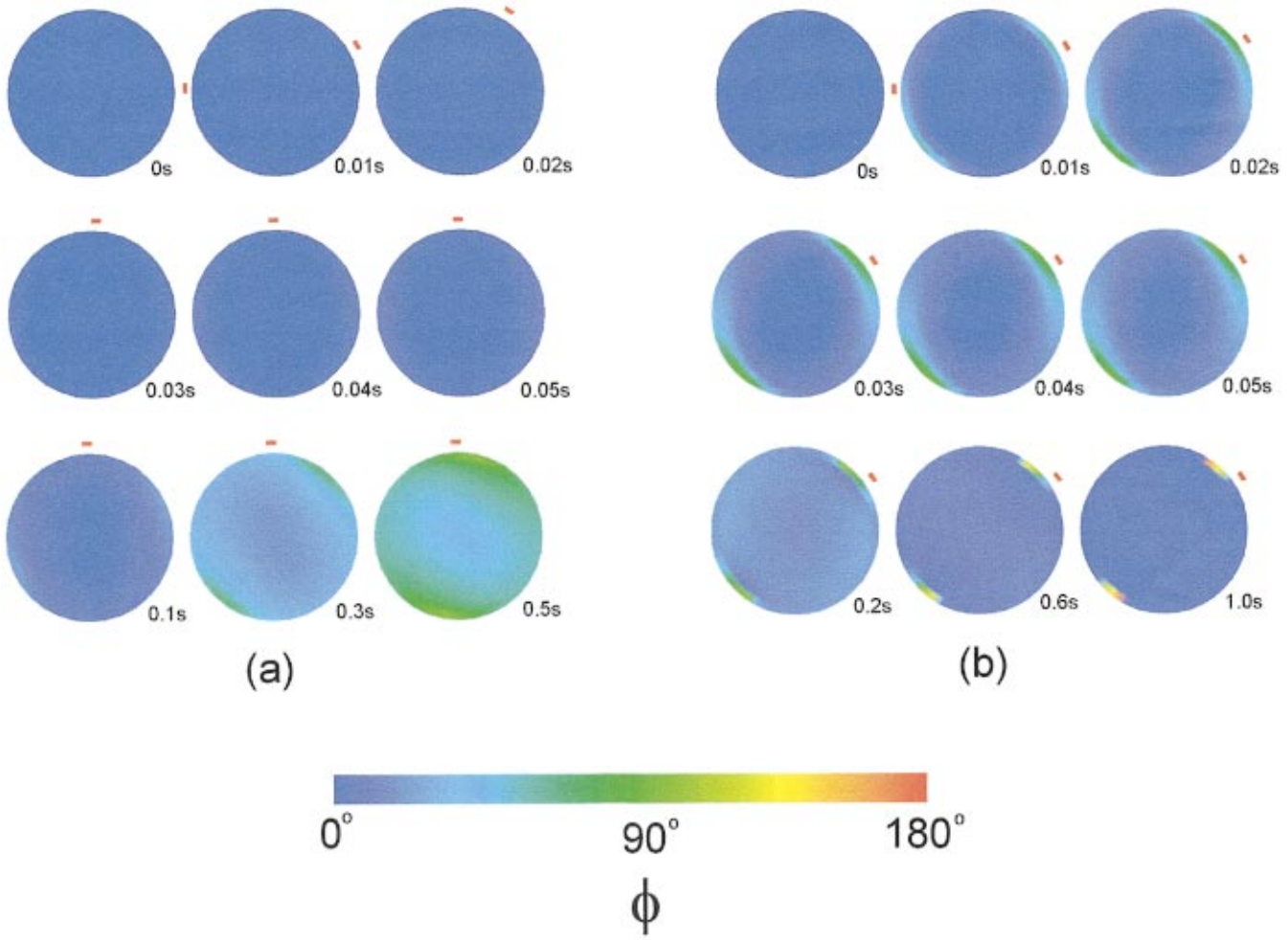

FIG. 4. (Color) Director patterns at different times for step-rotation pulses of 90° for $R=1$ mm (a) and 5 mm (b). Each circle shows the director pattern in the nematic sample at a given time, in scaled coordinates (cf. Fig. 1), using a false color representation of the director angle ϕ in each point of the sample. The red dot represents the amount of rotation of the tube at the same time. The shots are shown for times 0, 0.01, 0.02, 0.03, 0.04, 0.05, 0.1, 0.3, and 0.5 s for the case of $R=1$ mm and 0, 0.01, 0.02, 0.03, 0.04, 0.05, 0.2, 0.6, and 1.0 s for the case of $R=5$ mm.

continuous rotation. For this reason we shall still use Ω_c as a useful parameter to discriminate among different cases. We shall present simulations in conditions of continuous rotation, at various rotational speeds, for a ''standard'' geometry corresponding to a tube with a radius of 5 mm. We shall then apply our model to the exploration of step-rotation experiments, i.e., fast pulsed rotations of fixed angular amounts, in two geometries, characterized by a different radius of tube, namely, $R=1$ and 5 mm.

A. Continuous rotation

Let us first consider the case of a continuously rotating sample. A clear observation that can be inferred from calculations is that, if one neglects transient time dependence in the initial acceleration phase, the spatial dependence of the director distribution is relatively unimportant for low velocities (below the critical value), whereas it is relatively important for high velocities (above the critical value). The dependence upon the dimension of the sample is in any case rather weak. We comment here on results only for the case of a sample with radius equal to 5 mm. The following conditions have been imposed: the system is initially still, $f(t)=0$; then a linear acceleration is imposed on the system, $0<f(t)<1$, lasting a finite time of 0.001 s; finally, the system is kept in motion at constant speed Ω, i.e., $f(t)=1$. The sequence of times is chosen to mimic a ''realistic'' experimental situation, although other sequences could well be used, like a smoothly accelerating velocity profile.

We shall visualize the results of the simulations in terms of a director spatial distribution, i.e., as a map of the director field orientation in the sample. For a given time, a false color representation is used to visualize the director distribution: the color map associates values of ϕ with colors, ranging from 0° (blue), through 45° (cyan), 90° (green), 135° (yellow), to 180° (red). A red dot indicates, with its position, the amount of (counterclockwise) rotation of the sample at the chosen time. Figure 2 shows some chosen snapshots of the director distributions for $\Omega=\Omega_c/2$ [Fig. 2(a)] and $\Omega=2\Omega_c$ [Fig. 2(b)], i.e., half or twice the critical velocity. Not surprisingly, the predictions of the simplified treatment are confirmed, at least in the first case: for $\Omega=\Omega_c/2$ the system rapidly reaches a stationary state, with a homogeneous distribution close to $\phi=15°$, as predicted by Eq. (51). The critical velocity maintains its role of critical parameter, di-

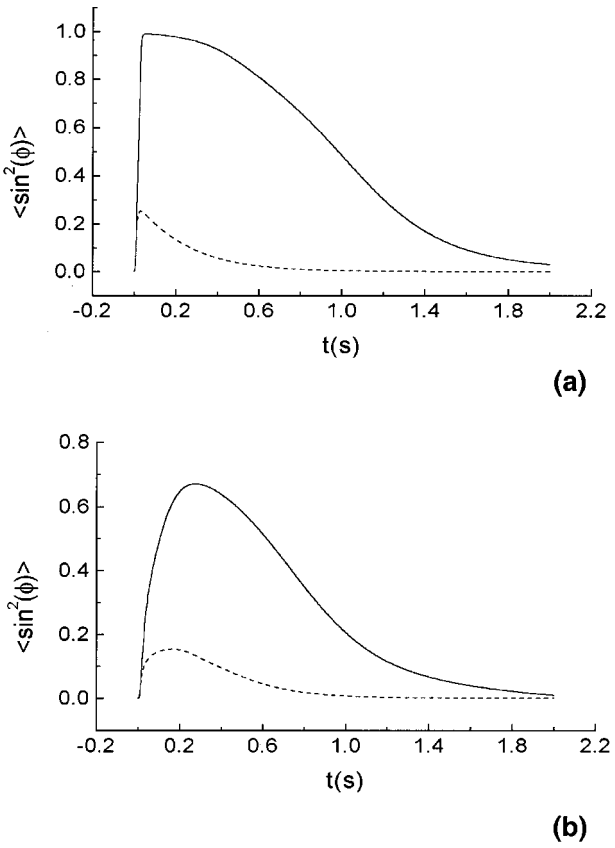

FIG. 5. Average value of $\sin^2\phi$ vs time for step-rotation experiments, $R=1$ mm (a) and 5 mm (b), with pulses 30° (dashed line) and 90° (full line).

viding stable solutions evolving to stationary conditions and unstable solutions. The solution shown for $\Omega=2\Omega_c$ is in fact characterized by director vortices, which are rapidly changing in time. The presence of unstable (oscillatory or otherwise) patterns in the director distribution for continuously rotating samples above the critical velocity is a relevant result which will be thoroughly explored in a following work. Here we would like to stress that (i) simplified standard treatments certainly cannot certainly account for these kinds of ''complex'' dynamical behaviors, which arise only in connection with a full exploration of the velocity-director coupling and (ii) although it is tempting to assume that patterns of this kind are produced in rotating samples during real experiments, it is necessary to consider the effect of different boundary conditions, order of magnitude of viscosity parameters, radius of the sample, initial conditions, and profile of the rotation velocity function. For instance, very high values of the viscosity numbers should lead to a rigidlike behavior of the director, with a homogeneous distribution of the director rotating in time, boundary conditions of Dirichlet type can lead to the creation of circular disclination at the boundaries [1], and so forth. Notice that, at least in the present set of calculated results, the velocity field in all cases reaches a stationary Newtonian behavior, i.e., $\psi=x^2/2$, after a transient time of the order of 0.01–0.1 s at most. The transient regime in continuous rotation experiments is equivalent to the first part of step-rotation experiments, and therefore the discussion of the velocity behavior at transient times is postponed to the next subsection.

B. Pulsed rotation

Next we shall consider simulated experimental conditions of step-rotation experiments, in which the system is subjected to a rapid rotational pulse of a given angle. In the following we shall treat the cases of pulses of 30° and 90°.

In Figs. 3 and 4 we show the calculated director patterns for the cases of samples of radius 1 and 5 mm and pulse angles of 30° and 90°. Simulations have been performed by first accelerating the system for 0.001 s, then rotating at constant speed for 0.01 (30°) or 0.03 s (90°), and finally decelerating the system for 0.001 s. The imposed rotational speed was in all cases equal to 50 rad s^{-1}. Again, the parametrization for the rotational pulse has been chosen to simulate realistically an experimental setup [7]. The results show clearly that a strong dependence on the dimension of the sample and the imposed rotation angle is present. For the case of radius equal to 1 mm [Figs. 3(a) and 4(a)] the system behaves more or less like a rigid system, except at very short times comparable to the pulse duration. The director exhibits a delay time in adjusting its orientation to the velocity field, but once the velocity field is stabilized the director reaches a stationary pattern, and, since the momentum of rotation is rapidly spread from the vessel walls to the whole sample in a time comparable to the pulse duration, the director rapidly reaches an almost uniform orientation close to the rotation angle. The relaxation to a state of alignment with the magnetic field then follows, in a much longer time scale that is comparable to the inverse of the critical velocity.

The director patterns for the case of large radius [Figs. 3(b) and 4(b)] show clearly the nonrigid and non-Newtonian behavior of the liquid crystalline fluid. The effect of the rotation is spread more slowly to the center of the sample and the dynamical evolution of the director and velocity fields takes place well beyond the duration of the pulse itself, when the rotation of the tube is stopped.

Analysis of the director patterns shows that in general during the fast rotation time the director starts to orient itself perpendicularly to the magnetic field from two areas corresponding to the maximum velocity (close to the borders) and at maximum angle with the initial director. These two areas rapidly grow to an annular region. When the cylindrical vessel ceases its rotation, the fluid is left under the influence of elastic and magnetic forces only, which causes the director to relax back to the original configuration aligned with the magnetic field. Notice that there is always a retardation effect, i.e., the director field change takes place at slower time scales than the velocity field evolution: thus the realignment to the field starts well beyond the time when the sample rotation is stopped.

By looking at the dynamic evolution of the director patterns we can therefore distinguish several time regimes in pulse step experiments. There is an initial short time t_{acc} characterized by a fast adjustment of the velocity field at the boundaries from the initial zero value to the stationary condition; in this first phase the velocity does not have any direct influence on the director reorientation, except in a region close to the boundaries, where the director starts to depart from the initially aligned distribution; t_{acc} is close in magnitude to the duration of the acceleration part of the rotation pulse, i.e., in our case of the order of 0.001 s. Next the director reorientation is spread to an annulus; this process

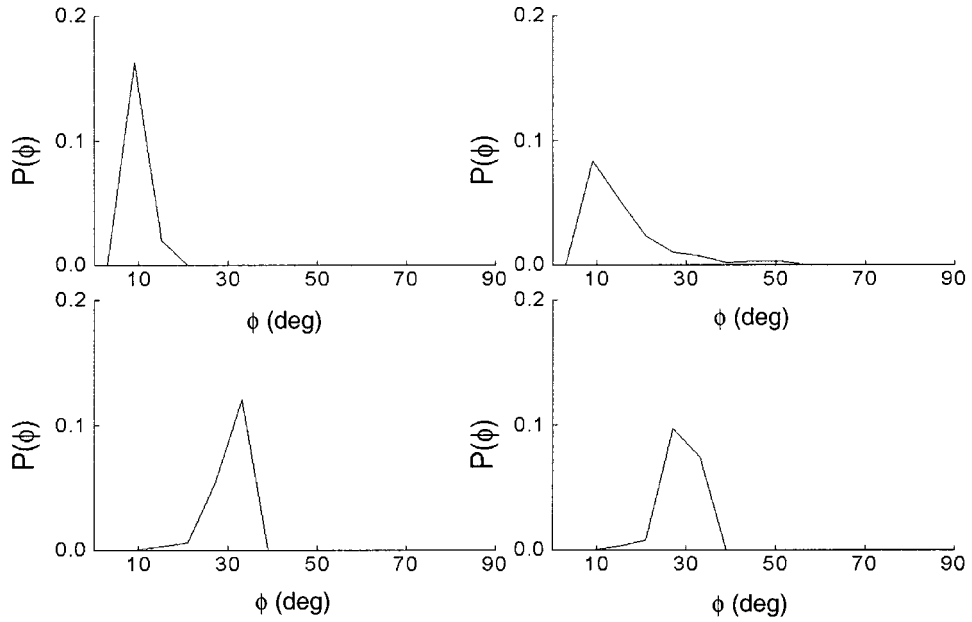

(a)

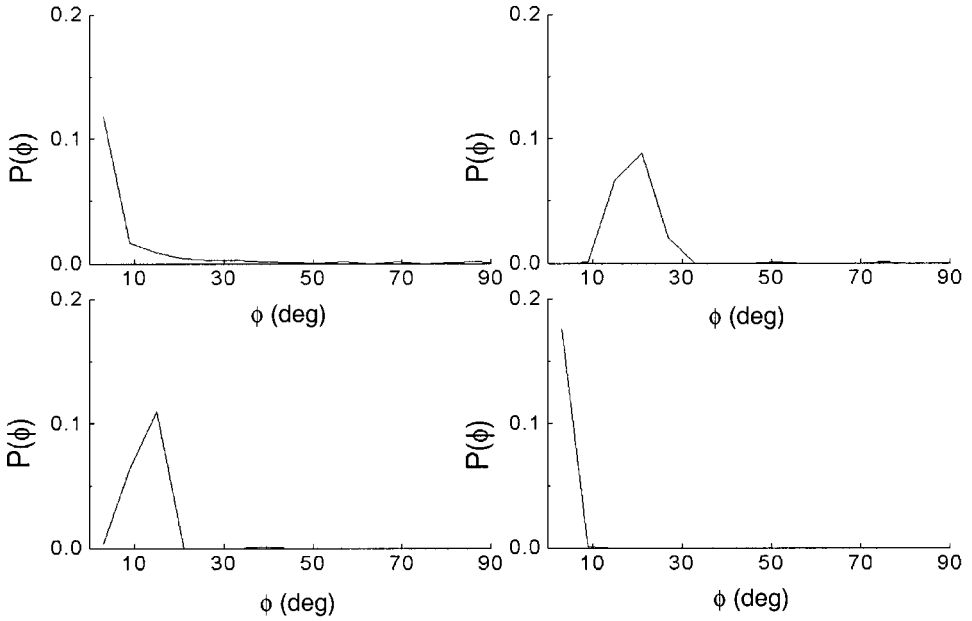

(b)

FIG. 6. Distribution $P(\phi)$ vs director orientation ϕ (in degrees) at different times for a pulse rotation of 30°; for $R=1$ mm (a) times are 0.01, 0.03, 0.05, and 0.5 s and for $R=5$ mm (b) times are 0.02, 0.2, 0.6, and 1.0 s.

seems to take place in a time t_{pulse} that is of the order of magnitude of the entire pulse duration, 0.01–0.03 s. After the tube has ceased its rotation, the region of realigned director field is spread to the rest of the sample in a time t_{spread} that depends on the sample dimension; it is very short for the small radius sample while it is at least ten times the duration of the pulse for the large radius sample, 0.1–0.2 s. Finally, the director starts relaxing back to the initial configuration aligned to the field, this process happening on a much longer time scale t_{relax}, roughly inversely proportional to the critical velocity, 1–2 s. Naturally, depending essentially upon the sample dimension and the angle of rotation, the director patterns are inhomogenously distributed in the sample [see Figs. 3(b) and 4(b)].

To support these general observations quantitatively, we show plots of $\langle \sin^2 \phi \rangle$ vs time for radius 1 mm in Fig. 5(a) and 5 mm in Fig. 5(b). The intrinsic ''rigidity'' of the small sample is evident: the director is reoriented rigidly during the

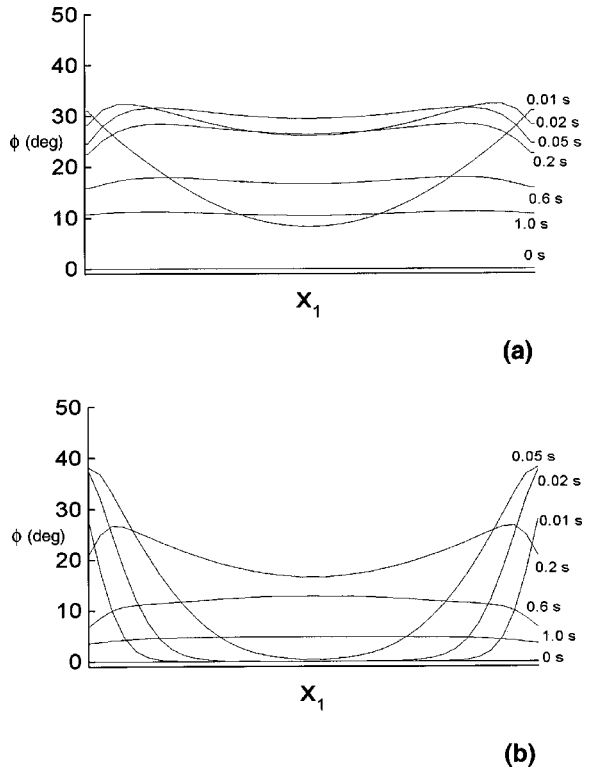

FIG. 7. Director angle ϕ vs x_1, i.e., along the horizontal diameter of the sample, for a pulse rotation of 30° and $R=1$ mm (a) and 5 mm (b). Times (in s) are reported in the figure.

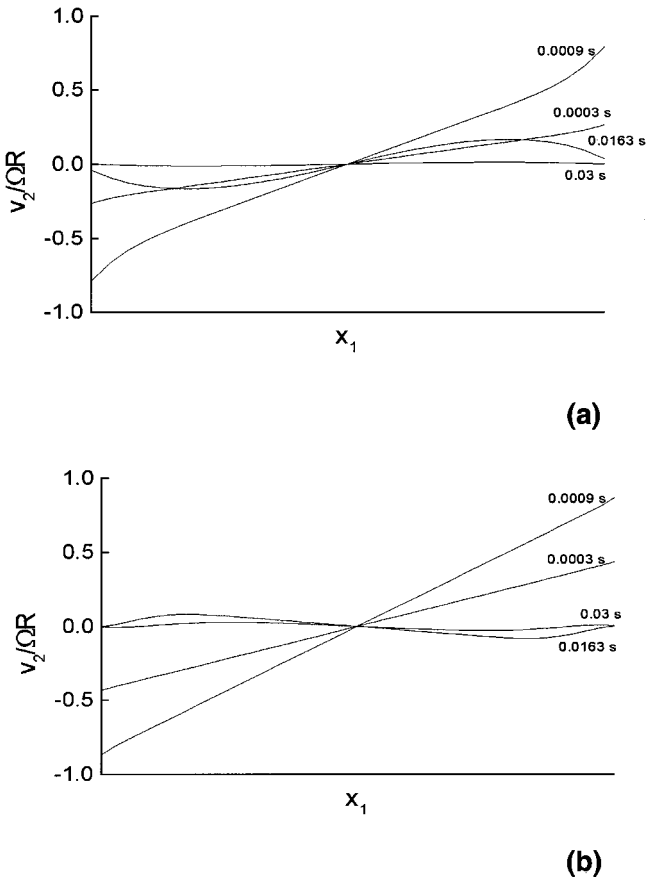

FIG. 8. Scaled component of the velocity field $v_2/\Omega R$ vs x_1 for a pulse rotation of 30° and $R=1$ mm (a) and 5 mm (b). Times (in s) are reported in the figure.

rotation pulse and it reaches a maximum displacement from the initial distribution which corresponds to the pulse angles 30 or 90°. The time t_{pulse}, which we can identify as the time required by the velocity field to reach a stationary state, covers the duration of the pulse; t_{spread} is very short. Afterward the system relaxes back to the initial configuration aligned with the magnetic field. For the larger radius sample t_{spread} is longer, and the system is unable to reach a maximum alignment equal to the rotation angle of the system. In other words, the director field in the bulk of the fluid is weakly influenced, during the short rotation of the tube: the system has an average orientation close to half the rotation angles in the three cases considered. The slow processes of realignment are essentially similar to the small radius case. Analogous information concerning the director orientation can be obtained from analyzing probability plots, i.e., distributions $P(\phi)$ at different times in the sample. In Fig. 6 we show a selection of distributions for four times (see the caption) for the case of a 30° pulse and radius 1 mm [Fig. 6(a)] and 5 mm [Fig. 6(b)]. Naturally, the local behavior of the director field can be analyzed in detail also by looking directly at the time evolution along sections of the sample or in defined areas. In Fig. 7 we show, for further comparison, the director field values along the horizontal diameter.

The velocity field of the nematic fluid can also be analyzed in detail. The main information we obtain from our simulations is that the general dynamics of the velocity field of a low viscosity nematic fluid is essentially of a Newtonian type, i.e., the general features of velocity profiles, averaged and local values, are interpreted in a satisfactory way by a Navier-Stokes behavior. Naturally, backflow effects are present due to the effect of the director reorientation upon the velocity dynamics, which are relevant especially during the spreading phase of the director $t_{\text{pulse}}<t<t_{\text{spread}}$ after pulse rotation, and at long times when the velocity field is sensing the slow relaxation of the director under the influence of the magnetic torque. The dynamical behavior of the velocity field is sketched in Fig. 8, where we show the scaled $v_2/\Omega R$ component at several times for the section along the horizontal diameter: notice that during the pulse rotation the behavior of the velocity is rather similar in the two samples, i.e., for very short times and large acceleration the system reacts more or less as a rigid body; the velocity backshot is then enhanced in the 5 mm sample after the pulse is terminated, although it is weakly present also in the 1 mm sample at longer times, not shown here, where the velocity is almost totally relaxed back to zero and residual fluxes are due only to the backflow effect induced by the slow director relaxation.

V. SUMMARY

The purpose of this work was to analyze the dynamical behavior of a low viscosity nematic liquid crystal in a rotating cylinder in the presence of a magnetic field, as described by Leslie-Ericksen equations for the coupled director and velocity fields, through a full numerical solution confined to two dimensions.

A computational methodology has been presented to describe different experimental setups, defined by suitable pro-

files of the rotational speed imposed on the cylindrical vessel. In particular, we have analyzed the director patterns of a continuously rotating sample and several cases of step rotation, i.e., simulated experiments in which the rotation is imposed for a short duration at high velocities. We have chosen simplified boundary conditions equivalent to weak anchoring at the borders. We have shown that the velocity field is in general well described by a Navier-Stokes or Newtonian-like dynamics, whereas the director adjusts slowly under the influence of the velocity field distribution and of elastic and magnetic torques. It has been shown that the sample dimension is important in determining the rigidity of the director response: larger samples show the presence of transient inhomogeneous patterns, which are not present in smaller samples. The distribution of director orientations in the fluid has been shown to evolve in time from the initial homogeneous one to an intermediate inhomogeneous distribution, whose spatial dependence depends upon the sample dimension and the magnitude of the rotational velocity, and finally to relax back to a distribution aligned with the field.

In the case of a cylindrical vessel continuously rotating, we have shown that numerically exact solutions of the LE equations in two dimensions support standard predictions [1] based on simplified treatments of the director and velocity fields, at low rotational velocities. At high rotational velocities the director exhibits nonstationary patterns. For simulated step-rotation experiments, director patterns are created first as localized areas at the borders where the displacement between velocity and director field is maximum, then spread in an annular region, and finally inhomogeneously diffused to the whole sample.

Once time- and space-dependent solutions for the director field are available, it is possible to start quantitatively relating experimental evidence, coming especially from nuclear magnetic and electron spin resonance measurements, with the director patterns predicted by the hydrodynamic model. In the following paper, we shall discuss the interpretation of NMR spectra of nematics on the basis of the present complete numerical procedure and of approximate solutions.

ACKNOWLEDGMENTS

We acknowledge the financial support of the E.C. TMR Contract No. FMRX-CT97-0121. Support has also been provided by the Italian Ministry for Universities and Scientific and Technological Research (PRIN ex 40%), by the Italian National Research Council through its Centro Studi sugli Stati Molecolari and the Committee for Information Science and Technology and by the Portuguese Praxis XXI Contract No. 2/2.1/MAT/380/94. We would like to acknowledge the late Professor Pier Luigi Nordio, whose insight was essential in the initial stage of this research.

[1] P. G. de Gennes and J. Prost, *The Physics of Liquid Crystals* (Oxford University Press, Oxford, 1993), Chap. 3.
[2] S. Chandrasekhar, *Liquid Crystals* (Cambridge University Press, Cambridge, England, 1992), Chap. 3.
[3] F. L. Leslie, Arch. Ration. Mech. Anal. **28**, 265 (1968); Adv. Liq. Cryst. **4**, 1 (1979).
[4] J. L. Ericksen, Trans. Soc. Rheol. **5**, 23 (1961); Adv. Liq. Cryst. **2**, 233 (1976).
[5] V. Tsvetkov and A. Sosnowskii, Acta Physicochim. URSS **18**, 358 (1943).
[6] H. Gasparoux and J. Prost, Phys. Lett. **36A**, 245 (1971).
[7] F. M. Leslie, G. R. Luckhurst, and H. J. Smith, Chem. Phys. Lett. **13**, 368 (1972).
[8] J. W. Emsley, S. K. Khoo, J. C. Lindon, and G. R. Luckhurst, Chem. Phys. Lett. **77**, 609 (1981).
[9] H. Kneppe and F. Schneider, J. Phys. E **16**, 512 (1984).
[10] A. F. Martins, P. Esnault, and F. Volino, Phys. Rev. Lett. **57**, 1745 (1986); P. Esnault, J. P. Casquilho, F. Volino, A. F. Martins, and A. Blumstein, Liq. Cryst. **7**, 607 (1990); L. N. Gonçalves, J. Figueirinhas, C. Cruz, and A. F. Martins, *ibid.* **15**, 1485 (1993).
[11] P. Ziherl, M. Vilfan, and S. Žumer, Phys. Rev. E **52**, 690 (1995).
[12] P. Ziherl and S. Žumer, Phys. Rev. E **54**, 1592 (1996).
[13] P. Palffy-Muhoray, A. Sparavigna, and A. Strigazzi, Liq. Cryst. **14**, 1143 (1993).
[14] A. D. Kiselev and V. Y. Reshetnyak, Mol. Cryst. Liq. Cryst. Sci. Technol., Sect. A **265**, 527 (1995).
[15] T. Tsuji and A. D. Rey, J. Non-Newtonian Fluid Mech. **73**, 127 (1997).
[16] N. G. Dolmatova and E. N. Kozhevnikov, Akust. Zh. **43**, 350 (1997) [Acoust. Phys. **43**, 300 (1997)].
[17] G. Porte, J. F. Berret, and J. L. Harden, J. Phys. II **7**, 459 (1997).
[18] P. K. Chan and A. D. Rey, Liq. Cryst. **23**, 677 (1997).
[19] A. Polimeno and A. F. Martins, Liq. Cryst. **25**, 545 (1998); A. Polimeno, L. Orian, P. L. Nordio, and A. F. Martins, Mol. Cryst. Liq. Cryst. Sci. Technol., Sect. A **336**, 17 (1999); A. Polimeno, L. Orian, P. L. Nordio, and A. F. Martins, *ibid.* (to be published).
[20] R. G. Larson and L. A. Archer, Liq. Cryst. **19**, 883 (1995).
[21] A. Chrzanowska and K. Sokalski, Phys. Rev. E **52**, 5228 (1995).
[22] A. Y. Zubarev and L. Y. Iskakova, Physica A **229**, 188 (1996).
[23] M. Kroger and S. Sellers, Phys. Rev. E **56**, 1804 (1997).
[24] M. Fialkowski, Phys. Rev. E **58**, 1955 (1998).
[25] F. Volino, Ann. Phys. (N.Y.) **22**, 1 (1997); F. Volino, H. Gerard, and G. Gebel, *ibid.* **22**, 181 (1997).
[26] M. Imai, H. Naito, M. Okuda, and A. Sugimura, Mol. Cryst. Liq. Cryst. Sci. Technol., Sect. A **259**, 37 (1995); **262**, 267 (1995).
[27] G. Cipparrone, D. Duca, C. Versace, C. Umeton, and N. V. Tabiryan, Mol. Cryst. Liq. Cryst. Sci. Technol., Sect. A **266**, 263 (1995).
[28] P. T. Mather, D. S. Pearson, R. G. Larson, D. F. Gu, and A. M. Jamieson, Rheol. Acta **36**, 485 (1997).
[29] E. Cappelaere and R. Cressely, Colloid Polym. Sci. **275**, 407 (1997).
[30] J. F. Berret, Langmuir **13**, 2227 (1997).
[31] V. Sequeira and D. A. Hill, J. Rheol. **42**, 203 (1998).
[32] U. Kuhnau, H. Schmiedel, and R. Stannarius, Mol. Cryst. Liq. Cryst. Sci. Technol., Sect. A **261**, 293 (1995).
[33] N. Yao and A. M. Jamieson, J. Rheol. **42**, 603 (1998).

[34] H. Gotzig, S. Grunenberghassanein, and F. Noack, Z. Naturforsch., Sci. Technol., Sect. A **261**, 283 (1995).
[35] M. Grigutsch, N. Klopper, H. Schmiedel, and R. Stannarius, Mol. Cryst. Liq. Cryst. Sci. Technol., Sect. A **261**, 283 (1995).
[36] E. Ciampi and J. W. Emsley, Liq. Cryst. **22**, 543 (1997).
[37] G. Althoff, N. J. Heaton, G. Grobner, R. S. Prosser, and G. Kothe, Colloids Surf., A **115**, 31 (1996).
[38] J. P. Casquilho, L. N. Gonçalves, and A. F. Martins, Liq. Cryst. **21**, 651 (1996).
[39] B. B. Diao and G. C. Berry, Liq. Cryst. **22**, 225 (1997).
[40] *Pattern Formation in Liquid Crystals*, edited by A. Buka and L. Kramer (Springer, Berlin, 1996).
[41] L. Landau and E. Lifsits, *Mécanique des Fluides* (Mir, Moscow, 1971).
[42] R. B. Bird, W. E. Stewart, and E. N. Lightfoot, *Transport Phenomena* (Wiley, New York, 1960), Chap. 3.
[43] B. Jerome, Rep. Prog. Phys. **54**, 391 (1991).
[44] A. C. Diogo and A. F. Martins, J. Phys. (France) **43**, 779 (1982).